

# Brief communication: Alternation of thaw zones and deep permafrost in the cold climate conditions of the East Siberian Mountains, Suntar-Khayata Range

Robert Sysolyatin<sup>1</sup>, Sergei Serikov<sup>1</sup>, Anatoly Kirillin<sup>1</sup>, Andrey Litovko<sup>1</sup> and Maxim Sivtsev<sup>1</sup>

<sup>1</sup>Melnikov Permafrost Institute, Yakutsk, 677000, Russia

*Correspondence to:* Robert Sysolyatin (robertseesaw@gmail.com)

**Abstract.** The Suntar-Khayata Range include numerous natural phenomena interacting or depending on permafrost conditions. Here, we examine some patterns of deep permafrost and talik zones on adjacent sites. A 210 m deep borehole in siltstone bedrock was equipped in July 2010 for temperature monitoring of the topmost 15 m and measurements of a deep permafrost temperature profile. The temperature curvature in the upper part has a bend which is consistent with at upper portion justify by climate warming and shows a steady-state linear geothermal profile below 85 m depth with a high geothermal heat flux. A shallow borehole situated at the river floodplain was used to investigate thaw zones temperature regime. Temperatures down to 6.7 m has been monitored at 5-min intervals during heavy rainfall and has had quite peculiar way. The thickness of the season freezing layer reach to 5.7 m, moreover ground temperature increases to 6 °C at 6.7 m depth by groundwater heat transfer. This study provides some new insight on the permafrost condition at one of the coldest places of Northern Hemisphere.

## 1 Introductions.

The East Siberian Mountains is one of the largest territory of east Siberia, but at the same time is researching how frontier permafrost region. On the other hand, the existing unique environmental conditions and natural cryosphere phenomena (glaciers, aufeis, “Pole of Cold” Oymyakon located at 63°15'N 143°9'E and Verkhoyansk located at 67°33'N 133°23'E e.g.) are interesting for the widespread scientific community (Lytkin and Galanin, 2016; Makarieva et al., 2022; Takahashi et al., 2011). Despite the increasing efforts in global permafrost mapping this area has almost no data on direct permafrost measurements and observations, which would be especially relevant in this data-scarce regions.

One of the main permafrost parameter is the permafrost thickness (Osterkamp and Gosink, 1991) which has considerably importance for paleo-climate reconstruction, hydrogeology description, deposit exploitation etc. The permafrost temperatures profile is controlled by initial surface temperature, bedrock thermal properties and geothermal heat flux (Lachenbruch and Marshall, 1986). Most frequently, the data about deep permafrost is acquired during geological-prospecting works for potential deposits. The expensive costs of deep borehole drilling limit its acquisition facilities, but in our case, we have access to a deep open borehole on gold ore deposit. In a previous study we focused on monitoring the active layer temperature regime by a widespread soil-pit network in an area close-by, but the temperature regime at the layer of zero annual amplitude (ZAA), season freezing layer as well as deep temperatures profiles have never been presented before (Sysolyatin et al., 2020).

In a cold climate with MAAT down to -12°C, taliks are almost certain to be avoided (Walvoord and Kurylyk, 2016). Since the heat balance of the subarctic is clearly not cold enough to induce talik formation, groundwater processes are more often involved. Taliks formed by thermal waters and open taliks (below large rivers) are well known, but taliks

37 confined to coarse-grained permeable sediments of riverbanks are poorly studied (Makarieva et al., 2019). Floodplain  
38 sediments can accumulate water during the warm period and gradually empty in the winter (Mikhailov, 2015). The  
39 occurrence of such taliks forms a favorable environment for the growth thermophilic plants out of their species range  
40 – e.g., poplar, willow shrub formation.

41 In this brief communication, we present the thermal regime of typical permafrost and talik sites at the Suntar-Khayata  
42 Range. The successful embedding of a shallow borehole allows to examine the active layer temperature evolution in  
43 a floodplain talik for the first time. We aim to: 1) describe the typical permafrost conditions by possess data and  
44 discuss the present temperature changes 2) infer the possible extent of talik zones, discuss the origin of their formation  
45 and show the impact of heavy rainfall to ground temperature regime and slope stability. This study presents the general  
46 permafrost conditions and discusses possible ways to improve the permafrost mapping of the East Siberian Mountains.

## 47 **2 Study area.**

48 The Suntar-Khayata Range is located at the southern boundary of the East Siberian Mountains and serves as a  
49 watershed between Aldan and Indigirka River basins (Fig. 1). At altitudes between 2000 m asl and 2959 m asl a glacial  
50 area is persisting, representing largest of present glaciation in Siberia – with about 195 glaciers cover 163 km<sup>2</sup>  
51 (Ananicheva et al., 2010). The study area is represented by alpine relief with the height of the peaks from 1550 to  
52 2031 m asl. The shallow borehole is located at the valley basin of Vostochnaya Khandyga River at 850 m asl (Fig.  
53 1d), and the deep borehole is located in the narrow V-shaped valley Vostochnaya Khandyga tributary at 1100 m asl  
54 altitude (Fig. 1c). Late Paleozoic sandstone, siltstone and clay slate are prevalent bedrocks of the mountain rock,  
55 whereas the valley sediments consist of coarse-grained alluvium strata (Sokolov et al., 2015). Kurums exist at the foot  
56 and middle part of the mountain slopes and has widespread distribution (Lytkin and Galanin, 2016) and boulders can  
57 reach up to 3 m in diameter.

58 The climate conditions recorded at a weather station 43 km away from to east of the study site (Vostochnaya,  
59 WMO24679), situated at 1288 m asl. The MAAT ranges from -15.3°C to -11.2°C, average percipitation is about 280  
60 mm and maximum annual snow thickness vary from the 16 to 60 cm for the 1966-2018 period. Direct air temperature  
61 observation around the borehole at the floodplain shown the existence of winter temperature inversion at altitudes  
62 between 800 and 1400 m asl (Sysolyatin et al., 2020). The flora is not very diverse. Dwarf Siberian pine is occupying  
63 the top part of slopes between 1400 and 1600 m asl and able to accumulate significant snow cover. Siberian larch is  
64 growing on gentle and steep slopes, flat surfaces reflecting the most severe permafrost conditions. The poplars have a  
65 limited extent, adjacent to the riverbank.

66 According to our soil-pit monitoring network (Sysolyatin et al., 2020), the mean annual ground temperature ranges  
67 from -1.1 to -10.6°C at 1 m depth, active layer vary from 0.5 to 2.7 m and mean ground surface temperature can drop  
68 to -31°C. No direct observation of precipitation or snow thickness are available for the study area, but its influence is  
69 obviously significant. For instance, in 2021 anomalous heavy rains gave rise to numerous debris flows and the  
70 appearance of debris avalanches as well as an abrupt change in the talik temperature regime (Supplementary material,  
71 Fig. 3).

## 72 **3 Materials and method**

73 The deep borehole was drilled for prospecting of the orogenic gold deposit prospecting by a geological company in  
74 1991. Organic material is almost absent and soil thickness does not exceed 0.5-0.8 m. Core samples (with marked  
75 depths interval) were stocked close to the drilling site, where 4 samples have been collected for laboratory studies. In

76 2010 the sintered ice plug in the topmost 5 m was redrilled for establishing a temperature monitoring site. In 2020,  
77 temperature measurements were made at intervals of 5 m for depths of 20 to 150 m and 10 m for depths between 150  
78 and 210 m using a movable high-precision negative temperature coefficient thermistor and multiconductor cable. To  
79 reduce the impact of convection, the hole was plugged by dense material.

80 The shallow borehole was drilled using a wheeled drilling rig in gravel alluvium sediments without core sampling.  
81 The hole was cased with a PVC pipe with inner diameter of 20 mm and the sensors were inserted at 1, 3, 5 and 6.7 m  
82 depths. The space around the casing was filled by sand and well cutting. The first attempt to drill a borehole in the  
83 floodplain was reaching to a depth of 12 m, but a failure of drilling tools halted the process. At end of July the stratum  
84 was relatively dry.

85 Ground temperatures were monitored continuously within the shallow and deep borehole down to 6.7 and 15 m for  
86 one and 9 years, respectively. Measurements were made every 4 h with TMC50-HD thermistors that were attached to  
87 four-channel Onset HOBO data loggers (U12-008 model). Air and ground surface temperatures (2 cm depth) were  
88 acquired for the shallow borehole site using a 2-channel data logger (U23-003). The operation design of the different  
89 logger systems situated at sites and in interior of the boreholes is shown in Table 1. Since the sensors installed in the  
90 deep borehole at 5 and 15 m, we report the mean annual ground temperature determine the offset of heat wave  
91 penetration from surface. In accordance with local climatic conditions and thermal properties of the bedrock, to  
92 account for an equal seasonal cycle, MAGT was calculated for the periods September-August and January-December  
93 for depths of 5 and 15 m, respectively. For the shallow boreholes, the data presented for the high-frequency logging  
94 period (every 5 min) from 31 July to 8 September are used trace the impact of heavy rain infiltration events on the  
95 subsurface thermal regime.

## 96 **4 Result**

### 97 *4.1 Permafrost temperature evolution*

98 At the V-valley site, only two of four sensors (5 and 15 m) have useful and reliable data for analysis (Fig 2a and b).  
99 The ground temperatures below 0°C were recorded for the whole monitoring period at 5 m depth. The observed  
100 average MAGT is -4.25 °C for both depths. The ground temperature evolution show a sinusoidal pattern with smooth  
101 drifting following the changing climate condition. At 5- and 15 m depth, the amplitude ranges from 6.2 to 0.6 °C,  
102 respectively, for the whole measurement period. The fluctuations of mean annual ground temperature did not exceed  
103 0.61 °C at 5 m and 0.26 °C at 15 m. The warming trend that has been highlighted for the 2010 to 2015 period was  
104 changing to equivalent cooling until 2019 at both depths. In accordance with the results presented, the ZAA depth  
105 might vary from 10.9 to 13.9 for a thermal diffusivity of around  $1.21\text{-}1.96\times 10^{-6}\text{ m}^2\text{ s}^{-1}$  by core samples. However, as  
106 far as the temperature altering should not up over to 0.1 °C by annual period, the ZAA layer has been exceed 15 m  
107 depth.

### 108 *4.2 Permafrost thickness and thermal conditions*

109 The permafrost thickness observed by these direct measurements does not exceed 205-210 m in the deep borehole at  
110 V-valley. A detailed temperature profile is presented in Fig. 2c. Below the assumed depth of ZAA (20 m), the  
111 permafrost temperature increases downwards with a gradient ranging from 0.01 to 0.038 °C<sup>-1</sup> m. From the whole  
112 temperature curve the mean gradient was calculated as 0.0214 °C<sup>-1</sup> m. The initial surface temperature ( $T_0=-5.25\text{ °C}$ ) is  
113 obtained by best-fit linear extrapolation from a depth interval of 85-160 m due to the uniform value of the gradient

114 (Lachenbruch and Marshall, 1986). The values for the temperature anomaly (offset value from linear fit) at 20 m ( $A_{20}$ )  
115 and 40 m ( $A_{40}$ ), were calculated as 0.70 and 0.39 °C, respectively.

#### 116 4.3 Talik temperature regime

117 A simple geomorphology sketch of the shallow borehole site is present in Figure 3a and an annual and monthly  
118 temperature-time series for the floodplain site are shown in Figure 3b and c, respectively. The pattern of the 1 m depth  
119 temperature evolution is consistent with the air and surface temperature evolution. Temperatures ranged from -6.3 to  
120 6.6 °C and from -13.7 to 20.7 °C, respectively. Surprisingly, the temperature variation at 3m depth has been smaller  
121 than for the sensors below, just from -2 to 1.6 °C. Refreezing at 3 m depth began at the end of January and the zero-  
122 curtain period is present from approximately the end of June to September, dividing the floodplain (overburden)  
123 sediments into to 3 zones – upper active layer, intermediate frozen layer and bottom permanent talik. The spike in  
124 Figure 3c is related to percolation of warm rainwater to 3 m depth, probably through casing tube. The most peculiar  
125 temperature behavior is found for the 5 and 6.7 m depth sensors, which is surely related to heat advection of ground  
126 water movement. Patterns of temperature changes at 5 m depth are more linear, whereas at 6.7 m it is more exponential.  
127 The maximum absolute temperature ranged between 4.4 °C (5 m) and 7.7 °C (6.7 m), while minimum temperatures  
128 oscillated between -0.2 °C (5 m) and 0.3 °C (6.7 m). The ground at a depth of 5 m remained unfrozen for more than  
129 75% of the time of the year. In an isopleth plot the talik appears below to 5.7 m and obviously continuous downward  
130 (Fig 3b). At an air temperature of -9.9 °C and MAGST of -1.8 °C the MAGT for the observation period (almost a  
131 year) is -1.1, -0.1, 1.1, 1.8 °C for depths of 1, 3, 5 and 6.7 m, respectively.

### 132 5 Discussion

133 Permafrost thickness is one of the major components of the cryosphere and has a close relation to geothermal heat  
134 flux. According to Balobaev et al. (1985) the Suntar-Khayat Range is characterised by high values of geothermal heat  
135 flux up to 0.08-0.10 Wm<sup>-2</sup> usually concentrating under narrow V-shaped valleys. Through numerous geothermal  
136 measurements at the next orogenic gold deposits (Nezhdaninskoye) specific patterns of thermal conditions were  
137 determined. Thus, the angle of inclination of the surface reduces the geothermal heat flux according to the equation:

$$138 \quad q = q_0 \cos \alpha \quad (1)$$

139 where  $q$  – calculated geothermal heat flux;  $q_0$  – initial geothermal heat flux,  $\alpha$  – slope angle.

140 The interaction between altitude and surface temperature has also been presented in previous studies and might  
141 decrease MAGST to -6.5°C at 1800 m asl mountain peaks (Sysolyatin et al., 2020). As mentioned above, MAGT at 5  
142 m depth have rather similar value to the ZAA temperature. By the steady-state equation (2) and expect the decrease  
143 of the ZAA temperature upon upward height, the permafrost thickness was calculated (Table 1) (Carslow and Jager,  
144 1959; Guglielmin et al., 2011). By core samples, bedrock effective thermal conductivity is 2.41 Wm<sup>-1</sup> K<sup>-1</sup> and  $q_0 =$   
145 0.052 Wm<sup>-2</sup> in permafrost body at base altitude surface level – 1100 m According to the orographic configuration of  
146 the study area, the permafrost thickness at local peaks 2000 m asl can reach to ~ 500 m.

$$147 \quad Z = T * \frac{\lambda}{q} + ZAA \quad (2)$$

148 where,  $Z$  – estimated permafrost thickness, m;  $T$  – temperature at the ZAA depth, °C;  $\lambda$  – effective thermal  
149 conductivity, Wm<sup>-1</sup> °C<sup>-1</sup>;  $q$  – geothermal heat flux in permafrost Wm<sup>-2</sup> (from equation 1).

150 Extrapolation of the linear portion of temperature curve to the surface result in significant differences to the current  
151 temperature curve from the initial MAGST features (Lachenbruch and Marshall, 1986). Two variants of changes are  
152 considered, a temperature change at the surface and a temperature change at the ZAA. For instance, assuming thermal  
153 diffusivity is  $1.6 \times 10^{-6} \text{ m}^2 \text{ s}^{-1}$ , the surface temperature shift around  $1.4 \text{ }^\circ\text{C}$  would be ongoing from 22 to 81-year respect  
154 to step, linear or exponential way of changes. When the temperature shifts by  $0.7^\circ\text{C}$  at the ZAA, the response time  
155 will expand to a range of 19 to 90 years. With the available data about the rate of air temperature change at the closest  
156 weather station, the second variant is the most plausible. It should be noted that the snow cover can change the surface  
157 temperature by more than  $5 \text{ }^\circ\text{C}$  (Gisnas et al., 2014), which is much larger than the air temperature change over the  
158 last 80 years (IPCC, 2014).

159 As mentioned above, the talik appearance can only be caused by the thermal influence of superficial or ground water  
160 in the cold environments of northeastern Siberia. The absence of permafrost under large rivers and in the areas adjacent  
161 to hot springs is well-known. Nevertheless, in our case, where the distance from the main stream exceeds 1 km, the  
162 presence of the talik was not assumed before. The reason for the existence of the talik is ambiguous. One possibility  
163 is the migration of rainwater infiltrating through the "windows" of the kurums on the adjacent slope. The timing of  
164 the thermal impact of rainfall is clearly evident on the temperature graph at a depth of 1 m. These spikes have been  
165 well explained before (Hinkel et al., 2001). The divergent temperature response at depths of 5 and 6.7 m is difficult  
166 to explain, perhaps it may be related to the interaction of rainfall with the permafrost occurrence at depth. It could also  
167 have been due to a delay in the influence of groundwater supply from the river. However, the response time is largely  
168 consistent with the first hypothesis. The influence of groundwater from the river when considering the thawing cycle  
169 is certain. On the isopleth plot it is clearly shown that the temperature at the depth of 5 and 6.7 m begins to increase  
170 earlier than at a depth of 3 m, which means the proximity to the groundwater is accelerating warming for the coarse-  
171 grained sediments. To solve this issue, it would be necessary to install additional piezometric and temperature  
172 monitoring sites, as well as to carry out temperature measurements of the river water.

173 The features of floodplain taliks for Kolyma region are considered rather recently (Mikhailov, 2015). It is noted as the  
174 crucial reason for the formation of the winter river flow. Floodplain taliks of the region are capable to accumulate  
175 huge amounts of water and gradually return it back to the river during low-flow cold season. The main influencing  
176 factors are the slope of the river floodplain and the permeability of the sediments. Probably the reason for the  
177 appearance of such a large talik is just related to the site-specific conditions of the study area. A sufficiently reliable  
178 marker may be the areal of poplar trees, tending to warmer environments. However, in our case, at the drilling site the  
179 vegetation was represented by mosses and larch that is more typical for permafrost landscapes.

180 An increase in liquid precipitation, along with increase in air temperature, is one of the most obvious consequences  
181 of global warming (Savelieva et al., 2000; Yang et al., 2005). For the permafrost zone, heavy rainfall often acts as a  
182 trigger for geomorphological processes (Borgatti and Soldati, 2013). The effect of heavy rainfalls on permafrost is  
183 most pronounced for the mountainous areas.

184 The behavior of the upper part of the permafrost during flooding rains, creates reasons for the activation of slope  
185 processes. Heavy rains at the end of August 2021 were the trigger for 7 large landslides on a 5 km section of the  
186 Kolyma highway, temporarily stopping traffic (Supplementary material). The high concentration of landslides on this  
187 section is explained by the aspect and angle of the slope, creating favorable conditions for an increase of the active  
188 layer. Abrupt and abundant saturation with rainwater led to critical weighting of soil material, after which the stability  
189 of the slope has been disrupted. Landslide processes were also observed everywhere during field investigations in

190 other areas with a lower inclination and northern and eastern aspects. Descriptions of such scenarios are given in many  
191 sources, but the detailed process for regions of northeastern Siberia is poorly understood at this time (Frauenfelder et  
192 al., 2018; Geertsema et al., 2006; Gruber and Haeberli, 2007).

## 193 **6 Conclusion**

194 This study provides insight into thermal patterns of permafrost and talik that can be valuable for future studies of the  
195 East Siberian Mountains. Permafrost is almost continuously distributed with a thickness reach to 500 m. Thermal  
196 properties of the bedrock were obtained through laboratory determinations and a negligible permafrost temperature  
197 trend was identified as a result of long-term monitoring. Due to the successful location of the borehole and high-  
198 frequency measurements during rare heavy rains in August 2021, unusually high values of daily precipitation were  
199 recorded in the Suntar Khayata Mountains (Verkhoyansk Ridge, Siberia). Due to the abundance of liquid precipitation,  
200 peculiarities of the configuration of permafrost and thaw zones, as well as site morphology, the temperature regime  
201 of soils has a peculiar feature down to a depth of 6.7 m. The size of the talik zone can be very significant, which must  
202 be taken into account in mapping, design and modeling. A wide range of multidisciplinary research is required to  
203 improve the understanding of permafrost conditions in this area.

### 204 *Data availability*

205 The data are available from the authors upon request.

### 206 *Supplement*

207 Debris landslides evidence are added at Supplement material.

### 208 *Author contributions*

209 RG and SS proposed the initial idea and carried out this study by designing researching sites, analyzing data, and  
210 organizing and was responsible for the compilation and quality control of the observations. RG, SS, AL and MS  
211 handled with field works. AK responsible for laboratory determination of rock thermal properties. RG prepared the  
212 manuscript with contributions from SS, AK, AL and MS.

### 213 *Competing interests*

214 The authors declare that they have no conflict of interest.

## 215 **Acknowledgments**

216 This study has been funded by Republic of Sakha (Yakutia) and Russian Science Foundation (project N 22-27-20073).  
217 The authors acknowledge the Melnikov Permafrost Institute for logistic and field work support. Finally, we thank the  
218 reviewer Lutz Schirrmeister, anonymous reviewer, and editor Christian Hauck for comments and suggestions which  
219 helped improve the manuscript.

## 220 **References**

- 221 Ananicheva, M. D., Krenke, A. N. and Barry, R. G.: The Northeast Asia mountain glaciers in the near future by  
222 AOGCM scenarios, *Cryosph.*, 4(4), 435–445, doi:10.5194/tc-4-435-2010, 2010.
- 223 Balobaev, V. T., Devyatkin, V. N., Gavriliev, R. I. and Rusakov, V. G.: About geothermophysical researching of  
224 mineral deposits at north-east region, *Geol. Geol. Explor.*, 5, 36–37, 1985.

- 225 Borgatti, L. and Soldati, M.: 7.30 Hillslope Processes and Climate Change, in *Treatise on Geomorphology*, pp. 306–  
226 319, Elsevier., 2013.
- 227 Carslow, H. S. and Jager, J. C.: *Conduction of Heat in Solids*, Oxford University Press: New York., 1959.
- 228 Frauenfelder, R., Isaksen, K., Lato, M. J. and Noetzli, J.: Ground thermal and geomechanical conditions in a  
229 permafrost-affected high-latitude rock avalanche site (Polvartinden, northern Norway), *Cryosph.*, 12(4), 1531–1550,  
230 doi:10.5194/tc-12-1531-2018, 2018.
- 231 Geertsema, M., Clague, J. J., Schwab, J. W. and Evans, S. G.: An overview of recent large catastrophic landslides in  
232 northern British Columbia, Canada, *Eng. Geol.*, 83(1–3), 120–143, doi:10.1016/j.enggeo.2005.06.028, 2006.
- 233 Gisnas, K., Westermann, S., Schuler, T. V., Litherland, T., Isaksen, K., Boike, J. and Etzelmuller, B.: A statistical  
234 approach to represent small-scale variability of permafrost temperatures due to snow cover, *Cryosphere*, 8(6), 2063–  
235 2074, doi:10.5194/tc-8-2063-2014, 2014.
- 236 Gruber, S. and Haerberli, W.: Permafrost in steep bedrock slopes and its temperature-related destabilization  
237 following climate change, *J. Geophys. Res. Surf.*, 112(F2), doi:10.1029/2006jf000547, 2007.
- 238 Guglielmin, M., Balks, M. R., Adlam, L. S. and Baio, F.: Permafrost Thermal Regime from Two 30-m Deep  
239 Boreholes in Southern Victoria Land, Antarctica, *Permafr. Periglac. Process.*, 22(2), 129–139, doi:10.1002/ppp.715,  
240 2011.
- 241 Hinkel, K. M., Paetzold, F., Nelson, F. E. and Bockheim, J. G.: Patterns of soil temperature and moisture in the  
242 active layer and upper permafrost at Barrow, Alaska: 1993–1999, *Glob. Planet. Change*, 29(3–4), 293–309,  
243 doi:10.1016/S0921-8181(01)00096-0, 2001.
- 244 IPCC: *Climate Change 2014*, in *Synthesis Report, Contribution of Working Groups I, II and III to the Fifth*  
245 *Assessment Report of the Intergovernmental Panel on Climate Change*, p. 151, Geneva, Switzerland., 2014.
- 246 Lachenbruch, A. H. and Marshall, B. V.: Changing Climate: Geothermal Evidence from Permafrost in the Alaskan  
247 Arctic, *Science (80-. )*, 234(4777), 689–696, doi:10.1126/science.234.4777.689, 1986.
- 248 Lytkin, V. M. and Galanin, A. A.: Rock glaciers in the Suntar-Khayata Range, *Ice Snow*, 56(4), 511–524,  
249 doi:10.15356/2076-6734-2016-4-511-524, 2016.
- 250 Makarieva, O., Nesterova, N., Post, D. A., Sherstyukov, A. and Lebedeva, L.: Warming temperatures are impacting  
251 the hydrometeorological regime of Russian rivers in the zone of continuous permafrost, *Cryosph.*, 13(6), 1635–  
252 1659, doi:10.5194/tc-13-1635-2019, 2019.
- 253 Makarieva, O., Nesterova, N., Shikhov, A., Zemlianskova, A., Luo, D., Ostashov, A. and Alexeev, V.: Giant  
254 Aufeis—Unknown Glaciation in North-Eastern Eurasia According to Landsat Images 2013–2019, *Remote Sens.*,  
255 14(17), 4248, doi:10.3390/rs14174248, 2022.
- 256 Mikhailov, V. M.: Geographical regularities of distribution of floodplain taliks, *Izv. Ross. Akad. Nauk. Seriya*  
257 *Geogr.*, (1), 65, doi:10.15356/0373-2444-2014-1-65-74, 2015.
- 258 Osterkamp, T. E. and Gosink, J. P.: Variations in permafrost thickness in response to changes in paleoclimate, *J.*  
259 *Geophys. Res. Solid Earth*, 96(B3), 4423–4434, doi:10.1029/90JB02492, 1991.

260 Savelieva, N. ., Semiletov, I. ., Vasilevskaya, L. . and Pugach, S. .: A climate shift in seasonal values of  
261 meteorological and hydrological parameters for Northeastern Asia, *Prog. Oceanogr.*, 47(2–4), 279–297,  
262 doi:10.1016/S0079-6611(00)00039-2, 2000.

263 Sokolov, S. D., Tuchkova, M. I., Ganelin, A. V., Bondarenko, G. E. and Layer, P.: Tectonics of the South Anyui  
264 Suture, Northeastern Asia, *Geotectonics*, 49(1), 3–26, doi:10.1134/S0016852115010057, 2015.

265 Sysolyatin, R., Serikov, S., Zheleznyak, M., Tikhonravova, Y., Skachkov, Y., Zhizhin, V. and Rojina, M.:  
266 Temperature monitoring from 2012 to 2019 in central part of Suntar-Khayat Ridge, Russia, *J. Mt. Sci.*, 17(10),  
267 2321–2338, doi:10.1007/s11629-020-6175-3, 2020.

268 Takahashi, S., Sugiura, K., Kameda, T., Enomoto, H., Kononov, Y., Ananicheva, M. D. and Kapustin, G.: Response  
269 of glaciers in the Suntar–Khayata range, eastern Siberia, to climate change, *Ann. Glaciol.*, 52(58), 185–192,  
270 doi:10.3189/172756411797252086, 2011.

271 Walvoord, M. A. and Kurylyk, B. L.: Hydrologic Impacts of Thawing Permafrost-A Review, *Vadose Zo. J.*, 15(6),  
272 vzj2016.01.0010, doi:10.2136/vzj2016.01.0010, 2016.

273 Yang, D., Kane, D., Zhang, Z., Legates, D. and Goodison, B.: Bias corrections of long-term (1973-2004) daily  
274 precipitation data over the northern regions, *Geophys. Res. Lett.*, 32(19), n/a-n/a, doi:10.1029/2005GL024057,  
275 2005.

276

277

278

279

280

281

282

283

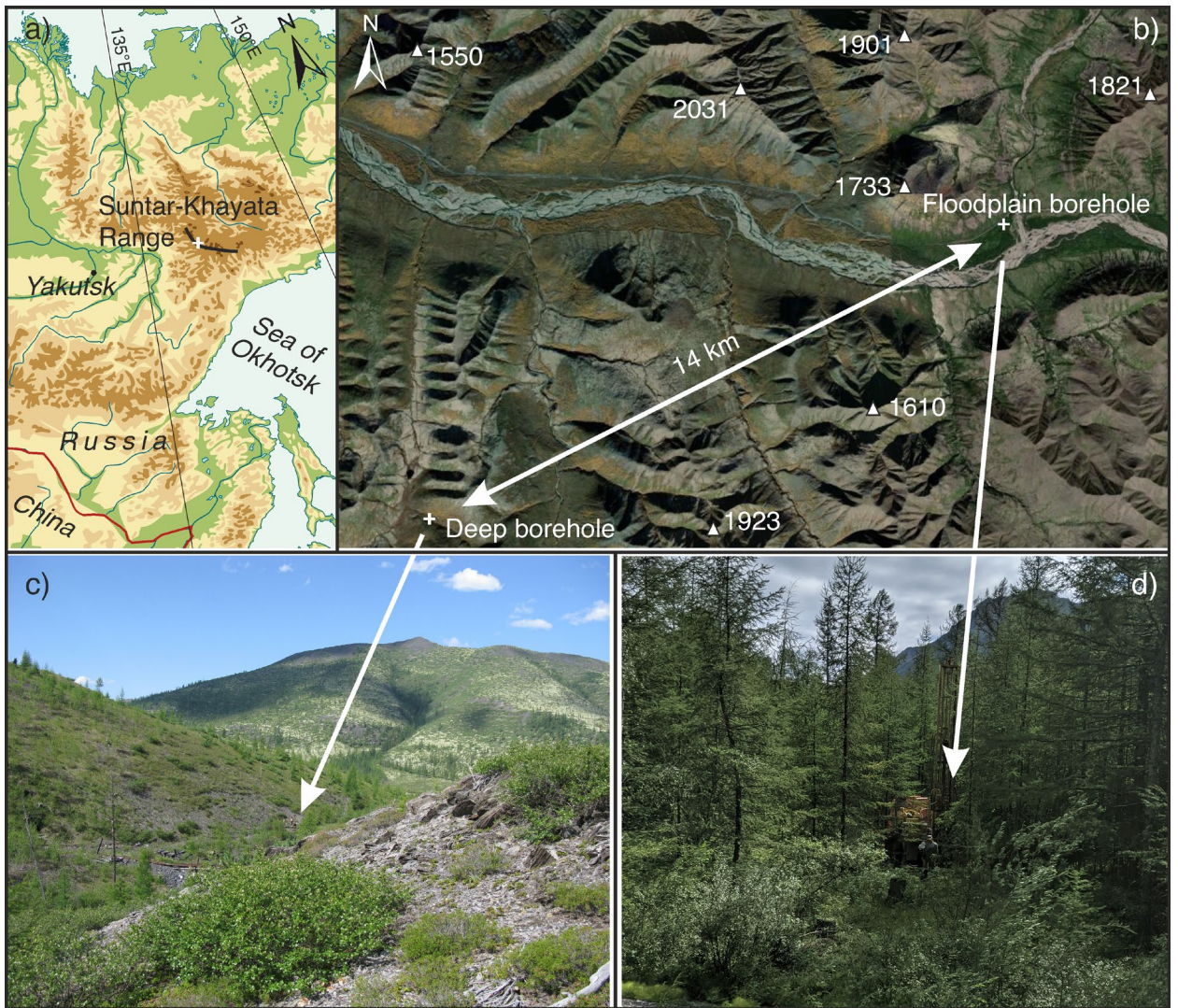
284

285

286

287

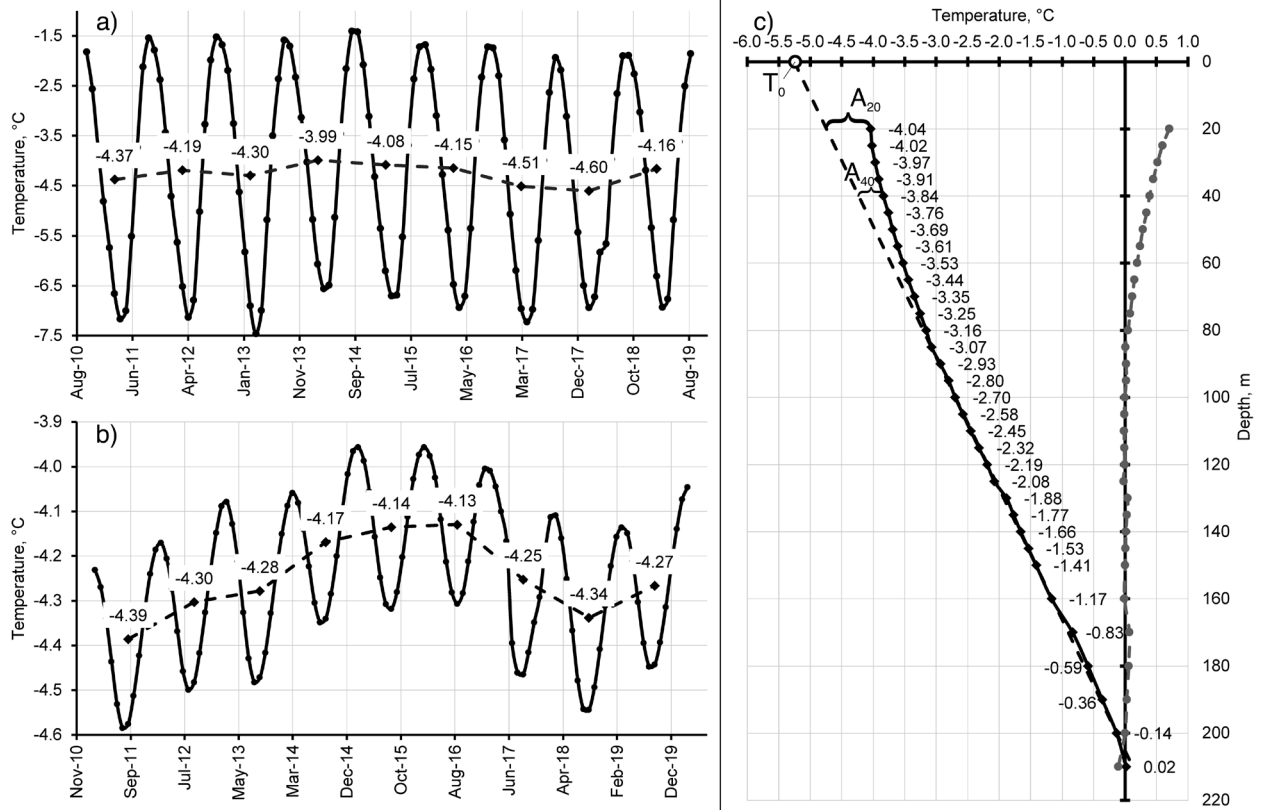




288

289 **Figure 1. Study area description and picture of sites environment. In (a) a modified physical map of the location of the study**  
 290 **area in eastern Siberia is shown (Map source: © GEOATLAS 1998). (b) MAXAR image of Vostochnaya Khandyga basin**  
 291 **with altitudes of peaks. (c) Deep borehole site at V-shaping valley. (d) Shallow borehole site at river plain.**

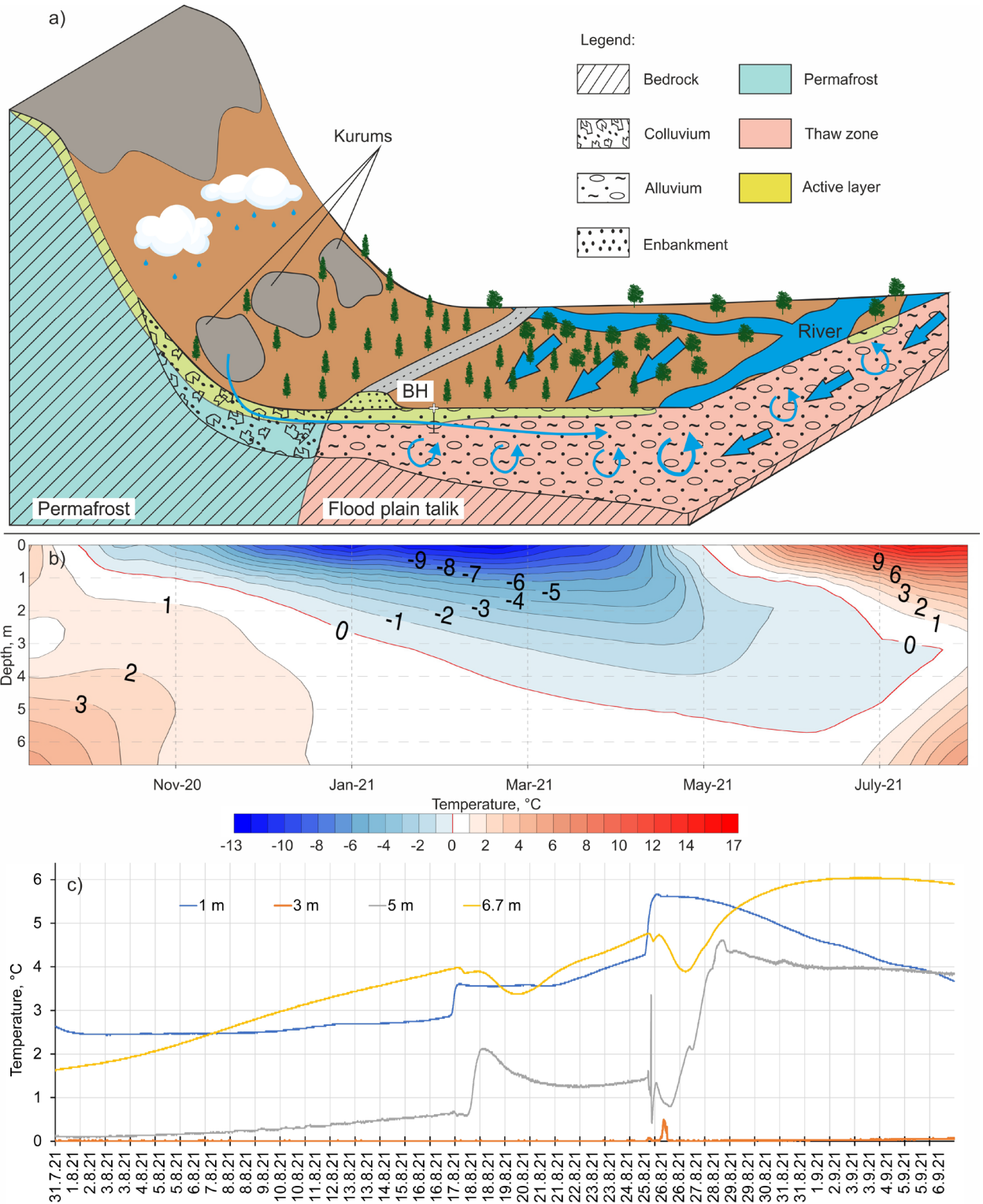
292



293

294 **Figure 2: Thermal regime of permafrost conditions in the deep borehole. Mean monthly and annual ground temperature**  
 295 **evolution at 5 m (a) and 15 m (b) depth. (c) Temperature profile (solid line), best linear-fit (dashed line) and current offset**  
 296 **from extrapolated temperature (dotted line).**

297



298

299 **Figure 3: (a) The scenario of ground water flow of the floodplain talik. (b) Annual ground temperature evolution and (c)**  
 300 **temperature fluctuation at a heavy rain event.**

301

302

303

304

305

Table 1

306 General parameters of equipment and operating timing of the loggers installed at different depths inside the  
 307 boreholes during the control period.

Location	Logger system and sensor	Accuracy and operation range	Sensor's depth, m	Measuring interval and operating time
River flood plain, Shallow borehole	OnSet Hobo U12-008	±0.25 °C at range -40 to 100 °C	1, 3, 5, 6.7	Every 5 min from 31-Jul-2021 to 7-Sep-2021/ Every 4 h from 8-Sep-2021 to 18-Aug-2022
River flood plain, Shallow borehole	OnSet Hobo U23-003		Air, Surface	
V-shaped valley, Deep borehole	OnSet Hobo U12-008		1*, 5, 10**, 15	Every 4 h from 20-Jul-2010 to 9-Sep-2021

308 \*non valid cause to close position to borehole's iron case tube

309 \*\*non valid because of misgiving temperature data at long period

310

311

Table 2

312 Permafrost thickness based on the assumption that MAGT and permafrost heat flow are decreasing under step-up of  
 313 peaks height.

Peak altitude, m	Slope inclination ( $\alpha$ ), grad	Cos $\alpha$	Temperature at ZAA (20 m depth), °C	q, Wm <sup>-2</sup> ,	Permafrost thickness, m
1550	24.2	0.912	-5.5	0.047	298
1600	26.6	0.894	-5.7	0.047	314
1700	31.0	0.857	-6.0	0.045	343
1800	35.0	0.819	-6.5	0.043	386
1900	38.7	0.781	-7.0	0.041	434
2000	42.0	0.743	-7.5	0.039	486

314